




Coherent seeding of the dynamics of a spinor Bose-Einstein condensate: From quantum to classical behavior

Bertrand Evrard , An Qu , Jean Dalibard , and Fabrice Gerbier

Laboratoire Kastler Brossel, Collège de France, CNRS, ENS-PSL Research University, Sorbonne Université, 11 Place Marcelin Berthelot, 75005 Paris, France



(Received 17 January 2021; accepted 12 February 2021; published 3 March 2021)

We present experiments revealing the competing effect of quantum fluctuations and of a coherent seed in the dynamics of a spin-1 Bose-Einstein condensate and discuss the relevance of a mean-field description of our system. We first explore a near-equilibrium situation, where the mean-field equations can be linearized around a fixed point corresponding to all atoms in the same Zeeman state $m = 0$. Preparing the system at this classical fixed point, we observe a reversible dynamics triggered by quantum fluctuations, which cannot be understood within a classical framework. We demonstrate that the classical description becomes accurate provided a coherent seed of a few atoms only is present in the other Zeeman states $m = \pm 1$. In a second regime characterized by a strong nonlinearity of the mean-field equations, we observe a collapse dynamics driven by quantum fluctuations. This behavior cannot be accounted for by a classical description and persists for a large range of initial states. We show that all our experimental results can be explained with a semiclassical description (truncated Wigner approximation), using stochastic classical variables to model the quantum noise.

DOI: [10.1103/PhysRevA.103.L031302](https://doi.org/10.1103/PhysRevA.103.L031302)

I. INTRODUCTION

The mean-field approximation is an essential tool of many-body physics. In this approach, the interaction of a single body with the rest of the system is treated in an averaged way, neglecting fluctuations around the mean and erasing any spatial correlations. The original many-body problem is then reduced to a much simpler one-body problem, a tremendous simplification enabling a basic analysis of the problem at hand. The accuracy of the averaging improves with the number of particles in direct interaction. Consequently, the mean-field treatment is well suited for highly connected systems, while important deviations are common for systems with short-range interactions in reduced dimensions.

When applied to bosonic quantum systems, a mean-field approach often entails another important approximation where intrinsic quantum fluctuations (and the correlations they induce) are neglected. Since quantum fluctuations are reflected in the noncommutativity of observables, field operators in the second-quantization formalism are replaced by commuting c -numbers. A possible improvement consists in replacing the field operators by classical stochastic fields [1–5], with a statistics properly chosen to be as close as possible to the original quantum problem. Such a semiclassical approach allows us to account quantitatively for quantum fluctuations while keeping the inherent simplicity of the mean-field equations.

In this Letter, we study the role of quantum fluctuations and the emergence of mean-field behavior in a quantum spinor Bose-Einstein condensate [6]. The atoms are condensed in the same spatial mode and interact all-to-all. The mean-field approach is thus well appropriate to study the dynamics in the spin sector, and has indeed been successfully used to describe

several situations, either at [7,8] or out-of [9–14] equilibrium. More recently, several experiments addressed the dynamics of a condensate prepared in an unstable configuration, achieving a high sensitivity to both classical and quantum fluctuations [15–31].

Here, our goal is twofold. First, we reveal the effect of quantum fluctuations in two different dynamical regimes, corresponding to persistent oscillations or relaxation to a stationary state [31]. Second, we address the relevance of a classical field description by comparing our experimental results systematically with three theoretical approaches. In the fully classical picture (C), we derive mean-field equations of motion and solve them for well-defined initial conditions, possibly including a coherent seed. In the semiclassical picture (SC), we keep the same mean-field equations of motion but for fluctuating initial conditions, with a probability distribution designed to model the quantum noise of the initial state. Finally, we perform a fully quantum treatment (Q), consisting in a numerical resolution of the many-body Schrödinger equation.

II. SPINOR BOSE-EINSTEIN CONDENSATES

We work with Bose-Einstein condensates of N spin-1 sodium atoms in a tight optical trap. Due to the strong confinement, all atoms share the same spatial wave function $\psi(\mathbf{r})$ [32], such that the spin is the only relevant degree of freedom. In this regime, the Hamiltonian describing the spin-spin interaction is (up to an additive constant) [6,32–34]

$$\hat{H}_{\text{int}} = \frac{U_s}{2N} \sum_{i,j=1}^N \hat{s}_i \cdot \hat{s}_j = \frac{U_s}{2N} \hat{\mathbf{S}}^2. \quad (1)$$

Here \hat{s}_i denotes the spin of atom i , $\hat{S} = \sum_i \hat{s}_i$ is the total spin, and U_s is the spin-spin interaction energy. In the single-mode limit, the spin-spin interaction is given by $U_s = (4\pi\hbar^2 a_s N/M) \int d^3\mathbf{r} |\psi(\mathbf{r})|^4$, where a_s is a spin-dependent scattering length, M is the mass of a sodium atom, and the spin-independent spatial mode ψ is the lowest energy solution of the time-independent Gross–Pitaevskii equation [35]. Note that technical fluctuations of the atom number N translate into fluctuations of U_s (other factors, such as fluctuations of the trap geometry, can also contribute to the latter). As will be discussed in more detail in Sec. IV, these technical fluctuations add to the intrinsic relaxation due to quantum fluctuations and thereby play a significant role in the interpretation of the experiments.

We use a magnetic field B aligned along the z axis to shift the energies of the individual Zeeman states $|m\rangle$, the eigenstates of \hat{S}_z with eigenvalues $m = 0, \pm 1$. Up to second order in B , the Zeeman Hamiltonian is $\hat{H}_Z = \sum_{i=1}^N p\hat{s}_{zi} + q\hat{s}_{zi}^2$, where $p \propto B$ and $q \propto B^2$ are the linear and quadratic Zeeman shifts, respectively. Noticing that $[\hat{S}_z, \hat{H}_{\text{int}}] = 0$, the first term in \hat{H}_Z is a constant of motion that can be removed by a unitary transformation. The total Hamiltonian thus reads [6]

$$\hat{H} = \hat{H}_{\text{int}} + \hat{H}_Z = \frac{U_s}{2N} \hat{S}^2 + q(\hat{N}_{+1} + \hat{N}_{-1}), \quad (2)$$

where \hat{N}_m is the number of atoms in $|m\rangle$.

Under a mean-field approximation, the annihilation operators \hat{a}_m are replaced by the c -numbers $\sqrt{N}\zeta_m = \sqrt{N_m} \exp(i\phi_m)$. By convention we set $\phi_0 = 0$, and we focus on the situation $S_z = 0$. We define the mean number of $(+1, -1)$ pairs $N_p = (N_{+1} + N_{-1})/2$, and take its normalized value $n_p = N_p/N$ and the conjugate phase $\theta = \phi_{+1} + \phi_{-1}$ as dynamical variables. In terms of these variables, the mean-field equations of motion are [9]

$$\hbar\dot{n}_p = -2U_s n_p (1 - 2n_p) \sin \theta, \quad (3)$$

$$\hbar\dot{\theta} = -2q + 2U_s (4n_p - 1)(1 + \cos \theta). \quad (4)$$

At $t = 0$, the BEC is prepared in a generalized coherent spin state $|\psi_{\text{ini}}\rangle = (\sum_m \zeta_{\text{ini},m} |m\rangle)^{\otimes N}$, with

$$\zeta_{\text{ini}} = \begin{pmatrix} \sqrt{n_{\text{seed}}} e^{i\frac{\theta_{\text{ini}} + \eta_{\text{ini}}}{2}} \\ \sqrt{1 - 2n_{\text{seed}}} \\ \sqrt{n_{\text{seed}}} e^{i\frac{\theta_{\text{ini}} - \eta_{\text{ini}}}{2}} \end{pmatrix}, \quad (5)$$

where $n_{\text{seed}} = N_{\text{seed}}/N$ and N_{seed} is the number of atoms in the $m = \pm 1$ states. The Larmor phase $\eta = \phi_{+1} - \phi_{-1}$ evolves as $\eta(t) = \eta_{\text{ini}} - 2pt/\hbar$ and does not play any important role in the following. We focus on the behavior of $N_p(t)$ as a function of time.

We notice that the state with all atoms in $m = 0$ (i.e., $N_{\text{seed}} = 0$ and hence $n_p = 0$) is stationary according to Eqs. (3) and (4). However, this state is not an eigenstate of \hat{H}_{int} and thus not a stationary state of the quantum equation of motion. In the absence of a seed, we identified in Ref. [31] two different regimes for the ensuing nonclassical dynamics:

(i) For $U_s/N \ll q$, the dynamics is reversible: The number of pairs $N_p(t)$ oscillates with a small amplitude.

(ii) For $q \ll U_s/N$, the dynamics is strongly damped and $N_p(t)$ relaxes to a stationary value.

Here, we revisit these experiments to investigate the effect of a coherent seeding of the $m = \pm 1$ modes.

III. REVERSIBLE DYNAMICS

A. Theoretical predictions

We focus first on the situation where $U_s/N \ll q \ll U_s$ and $n_{\text{seed}} \ll 1$. In this case, the reduced number of pairs n_p remains small at all times. Linearizing the mean-field Eqs. (3) and (4), we obtain [36]

$$N_p^{(C)}(t) \approx \frac{2U_s}{q} \sin^2(\omega t) \cos^2\left(\frac{\theta_{\text{ini}}}{2}\right) N_{\text{seed}}, \quad (6)$$

where $\omega \approx \sqrt{2qU_s}$. Note that the oscillation frequency ω is independent of the initial conditions θ_{ini} and N_{seed} . In Sec. IV, we investigate a regime where the frequency of the classical solution increases with N_{seed} , with dramatic consequences on the semiclassical dynamics.

To improve the prediction (6) and account for quantum fluctuations, we use a semiclassical approach: the truncated Wigner approximation [2–5,30]. The probability amplitudes $\zeta_{\text{ini},m}$ are treated as complex random variables which sample the initial Wigner distribution of the initial state at $t = 0$. The amplitudes are then propagated according to the mean-field equations of motion. Averaging the mean-field predictions over the fluctuations of ζ_{ini} , we find [30,36]

$$N_p^{(SC)}(t) \approx \frac{U_s}{2q} \sin^2(\omega t) \left[4 \cos^2\left(\frac{\theta_{\text{ini}}}{2}\right) N_{\text{seed}} + 1 \right]. \quad (7)$$

In analogy with quantum optics, the term $\propto N_{\text{seed}}$ in Eqs. (6) and (7) describes “stimulated emission” from the mode $m = 0$ to the modes $m = \pm 1$, while the additional term in Eq. (7) can be interpreted as “spontaneous emission.” We have verified numerically that the SC results are in good agreement with a fully quantum treatment. Moreover, comparing Eqs. (6) and (7), we notice that, unless the initial phase is chosen such that $\theta_{\text{ini}} \approx \pi$, a large seed $N_{\text{seed}} \gg 1$ makes the C and SC treatments almost identical, irrespective of the precise value of N . In fact, seeding with a few atoms $N_{\text{seed}} \approx 2-3$ and with $\theta = 0$ is sufficient to reach a 90% agreement between the two approaches.

B. Experimental sequence

We prepare a BEC in the state $m = 0$ using evaporative cooling in a crossed laser trap with a large magnetic field $B = 1$ G ($q \gg U_s$). After evaporation, the BEC contains $N \approx 2000$ atoms in the state $m = 0$, with $N_p \approx 100$ residual thermal atoms in $m = \pm 1$. We then turn on a strong magnetic-field gradient to pull the $m = \pm 1$ atoms out of the trap. After this purification step, we measure $N_p \ll 1$ [27].

We add a coherent seed using a combination of magnetic-field ramps and resonant radio frequency (rf) pulses. In a first step, a rf pulse is used to prepare the atoms in a coherent superposition with a probability n_{seed} to be in a given $m = \pm 1$ state. In a second step, the BEC is held in a large magnetic field, such that $q \gg U_s$ and θ_{ini} can be tuned, keeping $n_p = n_{\text{seed}}$ (see the Supplemental Material [36] for more details).

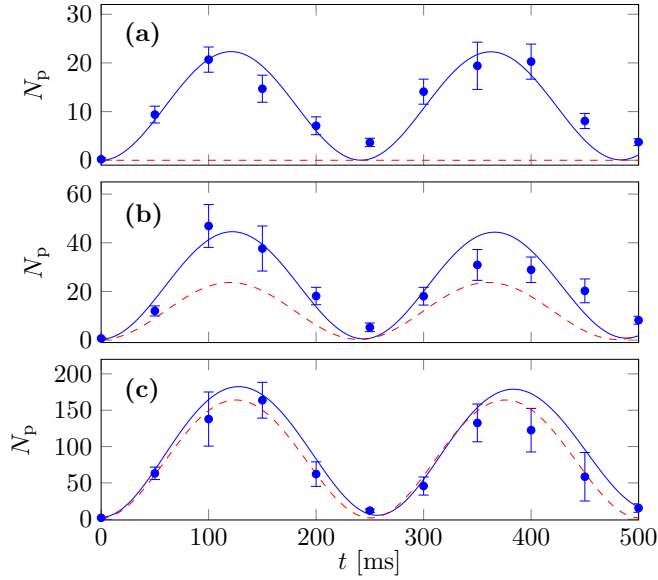


FIG. 1. Evolution of the number of $(+1, -1)$ pairs N_p (circles) for $q/h \approx 0.22 \pm 0.03$ Hz, $N \approx 1880 \pm 190$ atoms and various seed sizes: $N_{\text{seed}} \approx 0; 0.25; 1.8$ from panels (a) to (c). The initial phase is always set to $\theta_{\text{ini}} \approx 0$. The solid lines are numerical solutions of the Schrödinger equation with the many-body Hamiltonian in Eq. (2) using $U_s/h = 9.9$ Hz. The red dashed lines correspond to the classical prediction (6). Here and in the following, error bars show the statistical error corresponding to two standard errors.

In this way, we are able to prepare any coherent spin state given by Eq. (5), up to the phase η_{ini} , which is irrelevant for the experiments described here. The main imperfection in the preparation originates from the fluctuations of the total atom number $\delta N \approx 0.1N$, which induce $\approx 10\%$ relative fluctuations on N_{seed} . The magnetic field is then quenched to the desired value, and we let the system evolve for a time t before measuring the population of each Zeeman state using a combination of Stern-Gerlach separation and fluorescence imaging with a detection sensitivity around 1.6 atoms per spin component [27].

C. Experimental results

In Fig. 1, we show the time evolution of $N_p(t)$ for various initial states. In Fig. 1(a), we do not seed the dynamics. We observe an oscillation of $N_p(t)$, not captured by the classical description of Eq. (6) but in good agreement with the semiclassical predictions (7) or with the numerical resolution of the Schrödinger equation. In Fig. 1(b), we prepare a seed with $N_{\text{seed}} \approx 0.25 \pm 0.03$ (inferred from a calibration of the rf power) and $\theta_i \approx 0$. Compared with Fig. 1(a), the amplitude of the oscillations is doubled, in good agreement with Eq. (7). In Fig. 1(c), we set $N_{\text{seed}} \approx 1.8 \pm 0.2$ and $\theta_{\text{ini}} \approx 0$. The amplitude of the oscillations is further increased and now also well reproduced by the fully classical treatment (6). In all cases of Figs. 1(a)–1(c), the condition $N_p(t) \ll N$ remains fulfilled at all times. The validity of Eqs. (6) and (7) and the independence of the oscillation frequency on N_{seed} (as can be seen from Fig. 1) follow.

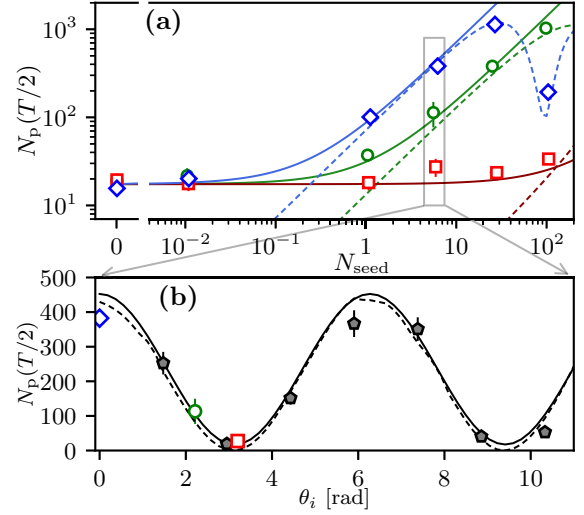


FIG. 2. (a) Number of pairs produced after half a period of evolution versus N_{seed} for $q/h \approx 0.33 \pm 0.03$ Hz and $N \approx 2920 \pm 280$. The blue diamonds, green circles, and red squares correspond to initial phases $\theta_{\text{ini}} \approx 0; 2.2; \text{ and } 3.3$ rad, respectively. For the three smallest seeds, N_{seed} is inferred from the calibration of the rf power. The solid lines are the semiclassical predictions given by Eq. (7) with $U_s/h \approx 12$ Hz, assuming $N_p \ll N$. For large N_{seed} , this approximation breaks down, but a numerical solution of the nonlinear classical mean-field (3) and (4) with fixed initial conditions becomes relevant. This fully classical treatment is shown as dashed lines. (b) Scan of the initial phase θ_{ini} after half a period of evolution for $N_{\text{seed}} \approx 6.0$.

We investigate the role of the initial phase θ_{ini} in Fig. 2. In Fig. 2(a), we plot the variation of $N_p(T/2)$, with $T = \pi/\omega$ the period of oscillations, against N_{seed} for three values of θ_{ini} . For $N_{\text{seed}} \ll 1$, we observe a saturation of $N_p(T/2)$ at a value independent of θ_{ini} , consistent with the SC prediction (7). For such small seeds, the dynamics is triggered by quantum fluctuations. For larger seeds, unless the antiphase-matching condition $\theta_{\text{ini}} \approx \pi$ is fulfilled (red curves), stimulated emission becomes dominant and the fully classical description is accurate. We observe a linear increase of $N_p(T/2)$ until the small-depletion approximation used to derive Eqs. (6) and (7) becomes inconsistent. For our data, this occurs for the point $N_{\text{seed}} \approx 100$, $\theta_{\text{ini}} \approx 0$. In this case, an exact resolution of the mean-field equations (3) and (4) provides accurate results. In Fig. 2(b), we set $N_{\text{seed}} \approx 6.0$ and scan the phase θ_{ini} . We measure oscillations of $N_p(T/2)$ in good agreement with Eqs. (6) and (7).

IV. RELAXATION DYNAMICS

A. Theoretical prediction

We now investigate the relaxation dynamics in a very small magnetic field, such that $q \ll U_s/N$. In this regime, the quadratic Zeeman shift q is negligible and we set it to zero for the calculation. However, the assumption $n_p \ll 1$ used to derive Eq. (6) is not valid and the mean-field Eqs. (3) and (4) cannot be linearized. For $q = 0$, the mean-field equations of motion can be solved directly. Taking for simplicity $\theta_{\text{ini}} = 0$,

we find [36]

$$n_p^{(C)}(t) = \frac{1}{4} - \frac{1 - 4n_{\text{seed}}}{4} \cos(\Omega t), \quad (8)$$

with an oscillation frequency

$$\Omega = \frac{4U_s}{\hbar} \sqrt{2n_{\text{seed}}(1 - 2n_{\text{seed}})}. \quad (9)$$

The nonlinear dependence of Ω with n_{seed} reflects the nonlinearity of the mean-field equations and has dramatic consequences when one takes into account quantum fluctuations. The seeds spontaneously created from the vacuum of pairs induce random shifts of the oscillation frequency around its mean-field value. Averaging over many realizations therefore results in an intrinsic dephasing of the oscillations predicted in Eq. (8). More precisely, for the generalized coherent spin state prepared in our experiment, the initial number of atoms in the $m = \pm 1$ modes $N_{+1,\text{ini}} + N_{-1,\text{ini}} = \Sigma$ follows a binomial distribution of mean $2N_{\text{seed}}$ (quantum partition noise). We use the random variable Σ as an initial condition to solve the mean-field Eqs. (3) and (4), i.e., substituting n_{seed} in Eq. (8) with $\Sigma/(2N)$. After averaging over the partition noise, we obtain for $N_{\text{seed}} \gg 1$ [36]

$$n_p^{(SC)}(t) \approx \frac{1}{4} - \frac{1 - 4n_{\text{seed}}}{4} \cos(\Omega t) e^{-\frac{1}{2}(\gamma_c t)^2}, \quad (10)$$

with a collapse rate

$$\gamma_c = \frac{2U_s}{\sqrt{N}\hbar} |1 - 4n_{\text{seed}}|. \quad (11)$$

The analytic formula (10) agrees very well with the numerical solution of the many-body Schrödinger equation for $N_{\text{seed}} \gtrsim 1$. The case $N_{\text{seed}} \ll 1$ can be treated using the truncated Wigner approximation [5] or an exact diagonalization of the interaction Hamiltonian (1) [31,37]. The dynamics also displays a relaxation of n_p to $1/4$, but with a different asymptotic behavior, $n_p - 1/4 \propto 1/t$. In a related work [38], it was shown that Poissonian fluctuations of the atom number in each mode of a two-component BEC caused a Gaussian decay of the two-time correlation function. For the spin-1 and two-component cases, a similar mechanism is at work. The combination of nonlinearities due to interactions and of quantum partition noise leads to dephasing and relaxation.

In an actual experiment, the relaxation of N_p is also enhanced by purely classical noise sources of technical origin. In our case, we identify shot-to-shot fluctuations of U_s (see Sec. II) as a significant additional mechanism contributing to the blurring of the oscillations. To account for this phenomenon, we average Eq. (10) over a Gaussian distribution of U_s with variance δU_s^2 . The resulting $n_p(t)$ has the same functional form as in Eq. (10) with the replacement

$$\gamma_c \rightarrow \Gamma = \sqrt{\gamma_c^2 + \gamma_t^2}, \quad (12)$$

with a technical blurring rate

$$\gamma_t = \frac{4\delta U_s}{\hbar} \sqrt{2n_{\text{seed}}(1 - 2n_{\text{seed}})}. \quad (13)$$

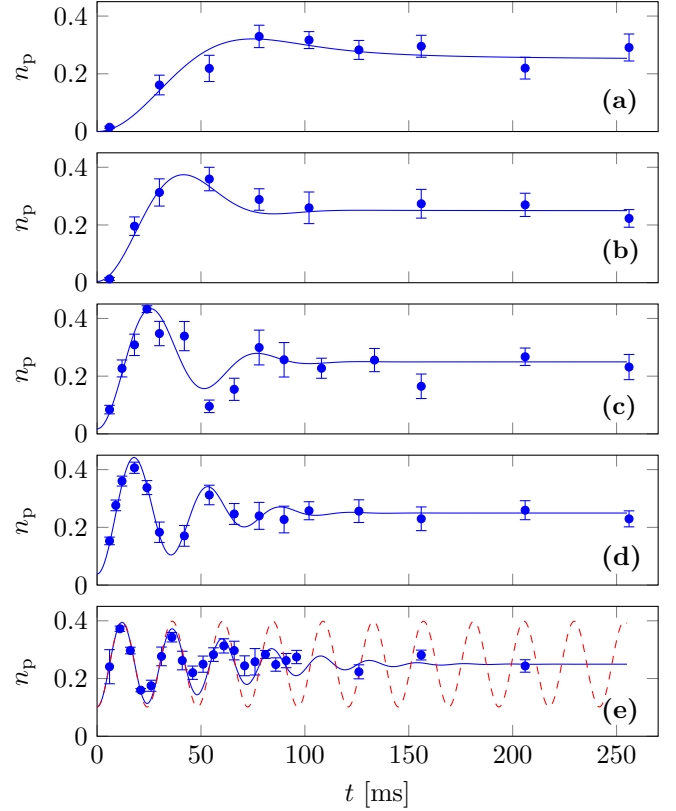


FIG. 3. Evolution of the fraction of $(+1, -1)$ pairs $n_p = N_p/N$ in a negligible magnetic field, for $N \approx 124 \pm 12$ atoms and various seedings: $N_{\text{seed}} = 0; 0.54; 2.1; 4.9; 12.8$; from panel (a) to (e). The initial phase is always set to $\theta_{\text{ini}} \approx 0$. The solid lines are numerical solutions of the Schrödinger equation for $U_s/\hbar = 24.5$ Hz. In panel (e), the red dashed line is the classical prediction from Eqs. (3), and (4).

For small enough seeds $n_{\text{seed}} \ll 1/4$, the total dephasing rate can be written

$$\Gamma \approx \gamma_c \sqrt{1 + 2 \left(\frac{2\delta U_s}{U_s} \right)^2 N_{\text{seed}}}. \quad (14)$$

This indicates a crossover from quantum to classical dephasing for seed sizes $N^* \approx U_s^2/(2\delta U_s)^2$.

B. Experimental considerations

To achieve the “zero field” regime $Nq \ll U_s$ experimentally, the best option is to reduce the atom number. Indeed, the density and therefore U_s cannot be arbitrarily increased due to undesired inelastic processes. Reducing the applied magnetic field further is not feasible due to ambient stray fields and environment-induced fluctuations (at the sub-mG level in our experiment). Therefore, we lower N by more than one order of magnitude with respect to the previous sections and prepare mesoscopic BECs of $N \approx 124 \pm 12$ atoms. We also slightly tighten the trap in order to achieve $U_s/\hbar \approx 24.5$ Hz. In this case, the central spatial density remains low enough to avoid inelastic collisions (more details in the Supplemental Material [36]).

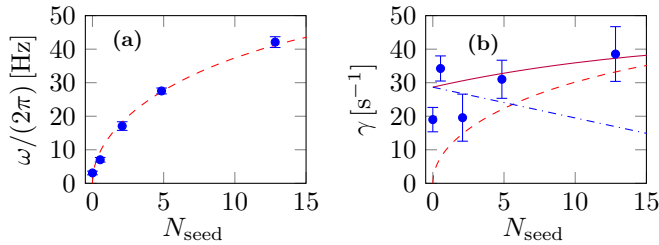


FIG. 4. (a) Frequency and (b) relaxation rate of the spin-mixing dynamics in a negligible magnetic field. The circles are obtained from a fit to the data of Fig. 3, with the error bars indicating the 95% confidence interval. In panel (a), the red dashed line corresponds to the frequency ω predicted by the mean-field treatment. In panel (b), the dash-dotted blue line corresponds to the rate γ_c of the collapse driven by quantum fluctuations, the red dashed line is the damping rate γ_t due to technical fluctuations, and the solid purple line corresponds to the total damping rate $\Gamma = [\gamma_c^2 + \gamma_t^2]^{1/2}$. We use the value $\delta U_s/U_s = 0.13 \pm 0.04$, obtained from a fit to the data.

C. Experimental results

We show in Fig. 3 the relaxation dynamics of n_p for various seed sizes n_{seed} . We observe an acceleration of the initial dynamics for increasing n_{seed} and the emergence of rapidly damped oscillations. Eventually, n_p relaxes to the stationary value $\approx 1/4$ in all cases. Numerical simulations with U_s taken as a fit parameter are overall in good agreement with the data, although they slightly underestimate the damping rate for the largest seed $N_{\text{seed}} = 12.8$.

To compare these experiments with the theoretical predictions, we fit a function of the form (10) to the data of Fig. 3, leaving Ω and Γ as free parameters. We report in Figs. 4(a) and 4(b) the fitted frequency and relaxation rate. The frequency is essentially insensitive to quantum or classical fluctuations, and the measured values agree well with the C or SC predictions. The relaxation rate varies little with N_{seed} in the range we have explored experimentally. This observation is explained by the SC theory including technical fluctuations. Indeed, the slow decrease of γ_c with N_{seed} is compensated by the increase of γ_t . Using $\delta U_s/U_s \approx 0.13$ as determined in

Fig. 4, we find a “quantum-classical crossover” for seed sizes around $N^* \approx 15$, close to the largest value we explored experimentally. For small seeds $N_{\text{seed}} \lesssim 5$, our measurements are consistent with a collapse driven primarily by quantum fluctuations. On the contrary, for the largest $N_{\text{seed}} \approx 12.8$, classical technical dephasing is the dominant damping mechanism.

V. CONCLUSION

We investigated the dynamics of a spin-1 BEC prepared with a majority of atoms in the Zeeman state $m = 0$ and possibly small coherent seeds in the $m = \pm 1$ modes. For a small but non-negligible magnetic field, we observe oscillations of the spin populations. This dynamics is triggered by quantum fluctuations in the absence of a seed and cannot be captured in a completely classical approach. Adding a coherent seed is phase-sensitive [30]. In general it corresponds to a dramatic increase of the oscillation amplitude, and the classical predictions become accurate as soon as a few atoms (typically $N_{\text{seed}} \gtrsim 2$) are used to seed the dynamics.

We also studied the dynamics in a negligible magnetic field. In this second regime, the combination of nonlinear mean-field equations and quantum noise leads to the relaxation of the spin populations. When the size of the seed increases, the intrinsic damping rate γ_c decreases and the mean-field picture becomes more and more relevant. However, it eventually fails for sufficiently long times. Experimentally, technical noise sources provide additional dephasing mechanisms of purely classical origin that can be completely described in the mean-field approach. In our experiment, we identify the fluctuations of the total atom number as the leading blurring mechanism when the seed size exceeds a dozen atoms.

All the experiments presented in this Letter are well captured by a semiclassical theory, where quantum fluctuations are modeled using stochastic classical variables. An interesting direction for future work would be to test experimentally the validity of such a semiclassical description in other contexts, in particular in a chaotic regime [31,39,40].

-
- [1] C. Gardiner and P. Zoller, *Quantum Noise* (Springer, Berlin, Verlag, 2004).
 - [2] A. Polkovnikov, *Ann. Phys. (NY)* **325**, 1790 (2010).
 - [3] M. J. Steel, M. K. Olsen, L. I. Plimak, P. D. Drummond, S. M. Tan, M. J. Collett, D. F. Walls, and R. Graham, *Phys. Rev. A* **58**, 4824 (1998).
 - [4] A. Sinatra, C. Lobo, and Y. Castin, *J. Phys. B: At., Mol. Opt. Phys.* **35**, 3599 (2002).
 - [5] R. Mathew and E. Tiesinga, *Phys. Rev. A* **96**, 013604 (2017).
 - [6] Y. Kawaguchi and M. Ueda, *Phys. Rep.* **520**, 253 (2012).
 - [7] W. Zhang, S. Yi, and L. You, *New J. Phys.* **5**, 77 (2003).
 - [8] D. Jacob, L. Shao, V. Corre, T. Zibold, L. De Sarlo, E. Mimoun, J. Dalibard, and F. Gerbier, *Phys. Rev. A* **86**, 061601(R) (2012).
 - [9] W. Zhang, D. L. Zhou, M.-S. Chang, M. S. Chapman, and L. You, *Phys. Rev. A* **72**, 013602 (2005).
 - [10] M.-S. Chang, Q. Qin, W. Zhang, L. You, and M. S. Chapman, *Nat. Phys.* **1**, 111 (2005).
 - [11] J. Kronjäger, C. Becker, M. Brinkmann, R. Walser, P. Navez, K. Bongs, and K. Sengstock, *Phys. Rev. A* **72**, 063619 (2005).
 - [12] J. Kronjäger, C. Becker, P. Navez, K. Bongs, and K. Sengstock, *Phys. Rev. Lett.* **97**, 110404 (2006).
 - [13] A. T. Black, E. Gomez, L. D. Turner, S. Jung, and P. D. Lett, *Phys. Rev. Lett.* **99**, 070403 (2007).
 - [14] Y. Liu, E. Gomez, S. E. Maxwell, L. D. Turner, E. Tiesinga, and P. D. Lett, *Phys. Rev. Lett.* **102**, 225301 (2009).
 - [15] C. Klempt, O. Topic, G. Gebreyesus, M. Scherer, T. Henninger, P. Hyllus, W. Ertmer, L. Santos, and J. J. Arlt, *Phys. Rev. Lett.* **104**, 195303 (2010).
 - [16] E. M. Bookjans, C. D. Hamley, and M. S. Chapman, *Phys. Rev. Lett.* **107**, 210406 (2011).

- [17] B. Lücke, M. Scherer, J. Kruse, L. Pezze, F. Deuretzbacher, P. Hyllus, J. Peise, W. Ertmer, J. Arlt, L. Santos *et al.*, *Science* **334**, 773 (2011).
- [18] C. D. Hamley, C. Gerving, T. Hoang, E. Bookjans, and M. S. Chapman, *Nat. Phys.* **8**, 305 (2012).
- [19] B. Lücke, J. Peise, G. Vitagliano, J. Arlt, L. Santos, G. Tóth, and C. Klempt, *Phys. Rev. Lett.* **112**, 155304 (2014).
- [20] D. Linnemann, H. Strobel, W. Muessel, J. Schulz, R. J. Lewis-Swan, K. V. Kheruntsyan, and M. K. Oberthaler, *Phys. Rev. Lett.* **117**, 013001 (2016).
- [21] D. Linnemann, J. Schulz, W. Muessel, P. Kunkel, M. Prüfer, A. Frölian, H. Strobel, and M. Oberthaler, *Quantum Sci. Technol.* **2**, 044009 (2017).
- [22] P. Kunkel, M. Prüfer, H. Strobel, D. Linnemann, A. Frölian, T. Gasenzer, M. Gärttner, and M. K. Oberthaler, *Science* **360**, 413 (2018).
- [23] M. Fadel, T. Zibold, B. Décamps, and P. Treutlein, *Science* **360**, 409 (2018).
- [24] K. Lange, J. Peise, B. Lücke, I. Kruse, G. Vitagliano, I. Apellaniz, M. Kleinmann, G. Tóth, and C. Klempt, *Science* **360**, 416 (2018).
- [25] T. Tian, H.-X. Yang, L.-Y. Qiu, H.-Y. Liang, Y.-B. Yang, Y. Xu, and L.-M. Duan, *Phys. Rev. Lett.* **124**, 043001 (2020).
- [26] H.-X. Yang, T. Tian, Y.-B. Yang, L.-Y. Qiu, H.-Y. Liang, A.-J. Chu, C. B. Dağ, Y. Xu, Y. Liu, and L.-M. Duan, *Phys. Rev. A* **100**, 013622 (2019).
- [27] A. Qu, B. Evrard, J. Dalibard, and F. Gerbier, *Phys. Rev. Lett.* **125**, 033401 (2020).
- [28] G. I. Mias, N. R. Cooper, and S. M. Girvin, *Phys. Rev. A* **77**, 023616 (2008).
- [29] X. Cui, Y. Wang, and F. Zhou, *Phys. Rev. A* **78**, 050701(R) (2008).
- [30] J. P. Wrubel, A. Schwettmann, D. P. Fahey, Z. Glassman, H. K. Pechkis, P. F. Griffin, R. Barnett, E. Tiesinga, and P. D. Lett, *Phys. Rev. A* **98**, 023620 (2018).
- [31] B. Evrard, A. Qu, J. Dalibard, and F. Gerbier, *Phys. Rev. Lett.* **126**, 063401 (2021).
- [32] S. Yi, Ö. E. Müstecaplıoğlu, C.-P. Sun, and L. You, *Phys. Rev. A* **66**, 011601(R) (2002).
- [33] T. Ohmi and K. Machida, *J. Phys. Soc. Jpn.* **67**, 1822 (1998).
- [34] T.-L. Ho, *Phys. Rev. Lett.* **81**, 742 (1998).
- [35] F. Dalfovo, S. Giorgini, L. P. Pitaevskii, and S. Stringari, *Rev. Mod. Phys.* **71**, 463 (1999).
- [36] See Supplemental Material at <http://link.aps.org/supplemental/10.1103/PhysRevA.103.L031302> for more details of the experimental sequence and the derivations of the theoretical results (6-14). The Supplemental Material includes Ref. [41].
- [37] C. K. Law, H. Pu, and N. P. Bigelow, *Phys. Rev. Lett.* **81**, 5257 (1998).
- [38] C. K. Law, H. Pu, N. P. Bigelow, and J. H. Eberly, *Phys. Rev. A* **58**, 531 (1998).
- [39] M. Rautenberg and M. Gärttner, *Phys. Rev. A* **101**, 053604 (2020).
- [40] J. Tomkovič, W. Muessel, H. Strobel, S. Löck, P. Schlagheck, R. Ketzerick, and M. K. Oberthaler, *Phys. Rev. A* **95**, 011602(R) (2017).
- [41] S. Uchino, M. Kobayashi, and M. Ueda, *Phys. Rev. A* **81**, 063632 (2010).